Hindawi Publishing Corporation
International Journal of Antennas and Propagation
Volume 2013, Article ID 426574, 12 pages
http://dx.doi.org/10.1155/2013/426574

Research Article

Spherical Helices for Resonant Wireless Power Transfer

Maja Škiljo and Zoran Blažević

University of Split, Faculty of Electrical Engineering, Mechanical Engineering and Naval Architecture, Ruđera Boškovića 32, 21000 Split, Croatia

Correspondence should be addressed to Zoran Blažević; zblaz@fesb.hr

Received 9 April 2013; Revised 1 July 2013; Accepted 6 July 2013

Academic Editor: Giuseppina Monti

The capabilities of electrically small spherical helical antennas for wireless power transmission at small and moderate distances are analyzed. Influence of design on antenna radiation resistance, efficiency, and mode ratio is examined. These are the factors that, according to the theoretical considerations depicted herein, govern the maximum transfer performances. Various designs and configurations are considered for the purpose, with accent on small-size receivers suitable for implementation in powering common-sized gadgets. It is shown that spherical helix design is easily manipulated to achieve a reduced antenna size. Good radiation characteristics and impedance match are maintained by multiple-arm folded antenna design and by adjusting the separation between the arms.

1. Introduction

Tesla's great experimental work at the turnover of XIX and XX centuries [1–6] was the first consideration in history of applying radio-waves and principle of resonant coupling on transmission of energy without wires. But only after the MIT experiment in 2007 [7] inspired by the couple-mode theory [8], there are serious efforts to commercialize small and midrange wireless power transfer (WPT) systems; see, for example, [9, 10]. The WPT technologies are adopted by the Wireless Power Consortium for the development and definition of standard Qi in 2009 for wireless charging, which is now implemented in portable consumer electronics. A survey of the WPT research history and commercial applications are summarized in [6]. The key to widespread application of the WPT principles is the optimization of the system regarding the transmission distance and efficiency. As already noted by Tesla, for an efficient resonant WPT in order for the maximum distance to be reached, the frequency of transmission should be as low as attainable. As this is practicable by using electrically small antennas (ESAs) only, there are problems of confining a large length of wire into a limited volume and the limited radiation efficiency of ESAs [2]. By applying the spherical mode theory antenna model on two equal ESAs in [11], it is shown that the lower the frequency and the greater the antennas' radiation efficiency are, the longer the maximum transmission range is.

The purpose of this paper is to address the problem of reducing the size of the antennas for WPT, depicted through examples of spherical helical antenna (SHA) design. SHA was originally proposed for the TRANSIT satellite for the positioning purposes prior to GPS [12]. It was chosen here for WPT over various ESAs for several reasons. Not only is it of convenient shape, but also the complete analytical solutions of electromagnetic (EM) field in form of the series expansion by spherical wave functions for a wide class of SHAs exist and are given in [13]. Moreover, spherical helix is analyzed by Wheeler in [14] too, where it is shown that a certain class of helical coils can be represented by an equivalent spherical coil, the results of which have also been verified analytically and experimentally in [15, 16]. Also, according to Wheeler [14] and [17], for the wire geometries that occupy equal electrical volumes in self-resonance, the larger the physical volume of the antenna, the shorter the wire needed to achieve the self-resonance. This is important for the WPT system design due to the ohmic loss problem that limits the radiation efficiency. It is shown in [18] that a significant improvement of radiation efficiency can be achieved by decreasing the temperature of the antenna conductors as in [3]. However, this requires the expedition of energy for

cooling. On the other hand, the comparison of the multiarm folded ESA with the inductively fed one in [19] proved that the former has a great potential for improving the radiation efficiency of ESAs by manipulating the design. The radiation properties of different types of multiple-arm folded helical antennas were investigated in [17, 20].

In this paper, the theoretical WPT performance bounds between two identical ESAs given in [11] are generalized to the case of different antennas. For that purpose, various SHA designs and configurations are compared by the radiation efficiency and the mode ratio match between the transmitter and the receiver. The analysis clearly shows that, besides the radiation efficiency, the mode ratio match between the antennas is another crucial factor for maximizing power transfer efficiency (PTE) defined as the ratio of the power delivered to the load and the total power that enters the transmitting antenna port [11]. This is important for all WPT systems that apply different antennas such as RFID, where there is still considerable space for improvement in performance related to the distance and reliability of reading tags. Moreover, even in the scenario of WPT between equal ESAs, the optimal frequency and the choice of antenna configuration are related to the spherical mode content of the EM field produced or received by the antenna, as shown in [21]. From that standpoint, the analysis of different single-arm and multiple-arm folded SHAs is performed in VHF band in order to assess the possibilities of maximizing WPT performances by the SHA design.

The paper is organized as follows. In Section 2, PTE between different antennas is analyzed; the maximum WPT efficiency bounds are derived, and the main factors governing the efficiency of the transmission are commented. The influence on the factors of the SHA antenna design is investigated in Section 3. It is found that, while decreasing the antenna size and attempting to maintain its radiation properties by adding folded arms as done in [15, 17–20], the decrement of the input resistance of electrically small SHAs can also be counteracted by decreasing the separation between the arms. In Section 4, the conclusions of the analysis are tested by comparisons of the results calculated by the antenna theory, simulated by FEKO [22] software, and measured in the laboratory by a vector network analyzer (VNA). The conclusions and aims of future work on the subject are given in Section 5.

2. The Optimization Parameters of Resonant WPT

Midrange resonant WPT system usually consists of ESAs, which generate predominantly the lowest-order spherical modes. It is shown in [11] that, by supposing a uniform current phase distribution across the antenna, the coupling between two reciprocal ESAs can be analyzed by applying the addition and translation theorem on the TE_{10} and TM_{10} modes. The assumption that there are no higher-mode interactions is not valid when two ESAs are very close to each other, but then the WPT efficiency is high even without proper receiver matching.

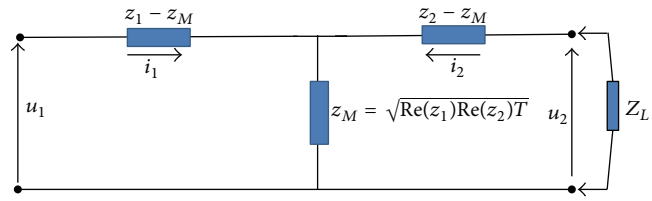

Figure 1: Equivalent scheme of WPT system.

The definition of ESA was first proposed by Wheeler [23] as an antenna whose maximum dimension is less than a "radian length" $\lambda/2\pi$. Chu [24] gave the equivalent definition of ESA as the antenna enclosed inside a "Chu sphere" satisfying the condition $ka < 0.5$, where $k = 2\pi/\lambda$ and $a$is the radius of a minimum sphere enclosed by the antenna. ESAs come close to the concept of the minimum scattering antennas (MSAs) [25] (or sometimes also referred to as the equal scattering antennas [26]). Such antennas have a property that, for the specific reactive termination at the antenna port, they do not scatter at all and thus become "invisible" for the transmitter. Should the termination be the open circle, the MSA is referred to as the minimum canonical scattering antenna. Furthermore, if the receiving MSA is matched, it scatters exactly the same power as that absorbed by the load. The analysis of coupling between two identical ESAs given in [11] can easily be extended to the case of different antennas by using the same approach and following [25]. The equivalent two-port network of two coupled ESAs is drawn as in Figure 1 accordingly.

According to the definition given in the Introduction section, PTE is calculated as in [11] by the following:

$$\mathrm{PTE} = \left|\frac{z_M}{z_2 + Z_L}\right|^2 \frac{\mathrm{Re}\left(Z_L\right)}{\mathrm{Re}\left(Z_{\mathrm{in}}\right)}, \tag{1}$$

where Z_{in} is the impedance seen at the input port of the transmitting antenna provided that the receiving antenna port is concluded by the impedance Z_L as follows:

$$Z_{\mathrm{in}} = z_1 - \frac{z_M^2}{z_2 + Z_L}, \tag{2}$$

$$z_{1,2} = R_{1,2}^{\mathrm{loss}} + R_{1,2}^{\mathrm{TM}} + R_{1,2}^{\mathrm{TE}} + j\,\mathrm{Im}\left(z_{1,2}\right) \tag{3}$$

are the free-space input impedances of the antennas (1 and 2) consisting of a reactive part, a loss resistance R^{loss}, and the radiation resistances R^{rad} of the spherical modes R^{TM} and R^{TE}. The mutual impedance z_M between the antennas is

$$z_M = \sqrt{\mathrm{Re}\left(z_1\right)\mathrm{Re}\left(z_2\right)}\mathbf{T}. \tag{4}$$

The transmission coefficient $\mathbf{T}$ between two different ESAs with the same orientation separated by the distance d is

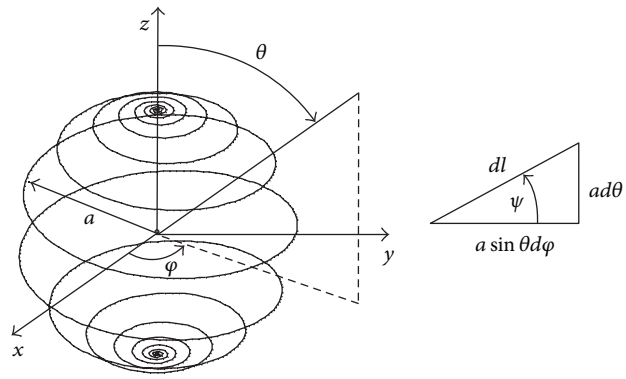

Figure 2: Basic SHA geometry.

derived by applying the addition and translation theorem of the spherical modes as follows:

$$\mathbf{T} = T_m \frac{3}{2} \left\{ \left(3\cos^2\vartheta - 1\right) \left[\frac{1}{(jkd)^3} + \frac{1}{(jkd)^2} \right] - \sin^2\vartheta \frac{1}{jkd} \right\} e^{-jkd}. \tag{5}$$

The term T_m is defined as a product of the radiation efficiency factor H_{T_m} and the mode ratio factor A_{T_m}:

$$T_m = H_{T_m} A_{T_m}. \tag{6}$$

Taking that the ESAs have the radiation efficiencies η_1 and η_2 and the spherical mode ratios α_1 and α_2, these factors are defined as the follows:

$$H_{T_m} = \sqrt{\eta_1 \eta_2}, \tag{7}$$

$$A_{T_m} = \frac{1 + \sqrt{\alpha_1 \alpha_2}}{\sqrt{(1 + \alpha_1)(1 + \alpha_2)}}. \tag{8}$$

Note that T_m is a function of the antenna design exclusively. The special case of (5) for equal antennas at transmission and reception ($A_{T_m} = 1$) is given in [11].

The optimal load $Z_L^{\text{opt}} = R_L^{\text{opt}} + jX_L^{\text{opt}}$ for which the maximum PTE between two different ESAs is obtained at a distance can be determined by the procedure given in [11]. First, the imaginary part X_L^{opt} is found as follows:

$$X_L^{\text{opt}} = \frac{1}{2} \operatorname{Re}[z_2] \operatorname{Im}\left[\mathbf{T}^2\right] - \operatorname{Im}[z_2], \tag{9}$$

and then the real part R_L^{opt} is given as follows:

$$R_L^{\text{opt}} = \operatorname{Re}[z_2] \sqrt{1 - \operatorname{Re}\left[\mathbf{T}^2\right] - \frac{1}{4}\operatorname{Im}^2\left[\mathbf{T}^2\right]}. \tag{10}$$

Note that the optimal load should be regarded as a function of the transmitter radiation efficiency and spherical mode ratio rather than of its input impedance, and so the maximum PTE obtained by inserting (9) and (10) into (1) should be as follows:

$$\text{PTE}_{\max} = \frac{|\mathbf{T}|^2}{2 - \operatorname{Re}\left[\mathbf{T}^2\right] + \sqrt{4\left\{1 - \operatorname{Re}\left[\mathbf{T}^2\right]\right\} - \operatorname{Im}^2\left[\mathbf{T}^2\right]}}. \tag{11}$$

With the frequency and distance given, it is a function of the T_m—term in (5) of the used antennas only. Hence, following (6)–(8), in order to achieve the maximum WPT performances, the antenna design should meet the requirement of maximizing radiation efficiency respecting the mode ratio match with the antenna that the energy is exchanged with. This puts some constraints on the antenna selection regarding different WPT scenarios, which are examined later in the following section.

3. Spherical Helical Antenna for WPT

The general geometry of a spherical wire can be described in terms of the functional relation of φ and θ; see Figure 2. The direction vector $\vec{l}$ is given by [13] as follows:

$$\vec{l} = \vec{\theta} + \sin\theta \frac{d\varphi}{d\theta} \vec{\varphi}. \tag{12}$$

There are various possibilities for winding a wire around a sphere, for example, with constant separation between the turns [27] or with constant separation between the wires [28]. In this paper, we focus on one particular function of $\varphi(\theta)$ defined in [13], which depicts the SHA geometry with the constant pitch angle ψ, where

$$\frac{d\varphi}{d\theta} = \frac{\cot\psi}{\sin\theta}. \tag{13}$$

Let us first consider a single-arm single-sensed SHA (SS-SHA) for the use in VHF band with radius $a = 8.75\,\text{cm}$ and pitch angle $\psi = 15.94^\circ$. The antenna is made of perfectly conducting (PEC) wire with radius $r_w = 0.05\,\text{mm}$. The simulations in FEKO simulation software are obtained using the method of moments (MoM). The unit voltage source is positioned in the middle of the center arm of the SHA. The upper diagram in Figure 3 shows that the open-ended single-arm SHA is in self-resonance at 162.3 MHz

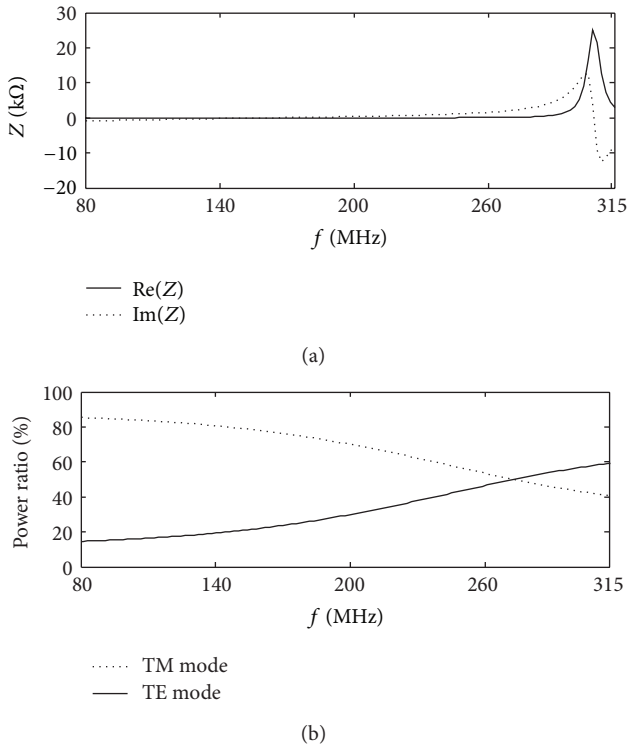

Figure 3: Impedance and power ratio of single-arm PEC SS-SHA.

and in antiresonance at 306 MHz. The percentage of the particular mode in the total power ($|E_\varphi/E_{\text{tot}}|^2$ and $|E_\theta/E_{\text{tot}}|^2$) depicted in the bottom in Figure 3 shows that the TM mode is dominant at low frequencies, whereas the TE mode starts to dominate over TM after 273 MHz, just before the antiresonance appears.

3.1. Multiple-Arm Folded SHAs. Depending on the SHA design, the adjustment of antenna radiation resistance can be accomplished in various ways, for example, by the multiple-arm folded SHA design [16, 22], or by more complex designs like the inductively fed four-arm SHA top-loaded monopole given in [29]. Multiple-folding method steps up the resonant radiation resistance when N_A identical folded arms are added in parallel to single-arm SHA and placed equidistantly on the sphere. Assuming equal currents induced along the arms, the radiation resistance increases with N_A^2, and loss resistance increases with a factor of N_A leading to high radiation efficiency [19].

Table 1 presents the SHAs where self-resonant frequency f_{res} and resonant radiation resistance are given for every PEC SHA with the number of arms N_A and the angle between the arms γ. Note that the SHAs are of equal arm lengths; that is, there is no change in the antenna geometry except for the increased number of arms. The first two sections show the results for SS-SHAs differing in distribution of angles between the arms. In the following text, EASS-SHA is referred to as even-angle (EA) SS-SHA, and CASS-SHA is referred to as closer-angle (CA) SS-SHA. The last section gives the results

Table 1: PEC SHAs' characteristics.

N_A/γ	f_{res} (MHz)	R^{rad} (Ω)
EASS-SHA		
1	162.3	5.3
2/180°	173.7	22.9
3/120°	181.0	54.3
4/90°	185.9	101.2
5/72°	189.3	159.7
6/60°	191.9	238.5
8/45°	195.5	437.4
CASS-SHA		
2/5°	169.6	22.7
3/5°	173.2	73.0
4/5°	175.7	136.2
6/5°	179.3	366.6
EARS-SHA		
1	172.6	5.0
2/180°	191.6	22.8
3/60°	201.8	58.9
4/90°	217.0	113.2
6/60°	228.4	326.1
CARS-SHA		
2/5°	181.0	22.8
3/5°	186.9	74.1
4/5°	191.3	140.0
6/5°	198.0	401.2

for reverse-sensed (RS) EA- and CA-SHAs referred to as EARS-SHA and CARS-SHA, respectively. The results show that the three-arm SHA design at considered frequencies is suitable for matching purposes in WPT. Therefore, we focus the following analysis on three-arm SHAs, but similar conclusions can also be derived for SHAs with a different number of arms. Figure 4 illustrates the examples of examined geometries, where the folded arms are rotated with respect to each other by the angles $\gamma = 120^\circ$ and $\gamma < 120^\circ$ for SS-SHAs and RS-SHAs, respectively.

The Smith impedance diagram in Figure 5 shows the variation of input impedance of one-, two-, and three-arm SHAs in the frequency span from 150 to 210 MHz describing a locus in the form of a circle. The Smith chart also shows the difference between the four examined SHA designs. As the number of folded arms increases, some observations can be noted. Due to the multiple-arm SHAs design where each antenna arm is shunted by another arm(s), the antiresonance occurs at the frequency lower than that of the self-resonance, and the inductive reactance dominates the SHA input impedance at the lowest frequencies. As noted in [17], the increase in internal capacitance between the folded arms caused the increase of self-resonant frequency. This is in agreement with the results in the Smith chart (Figure 5) where the increase in internal capacitance is observed as shifting the impedance circle slightly toward the domain of capacitive reactance, as in the RLC circuits shunted by

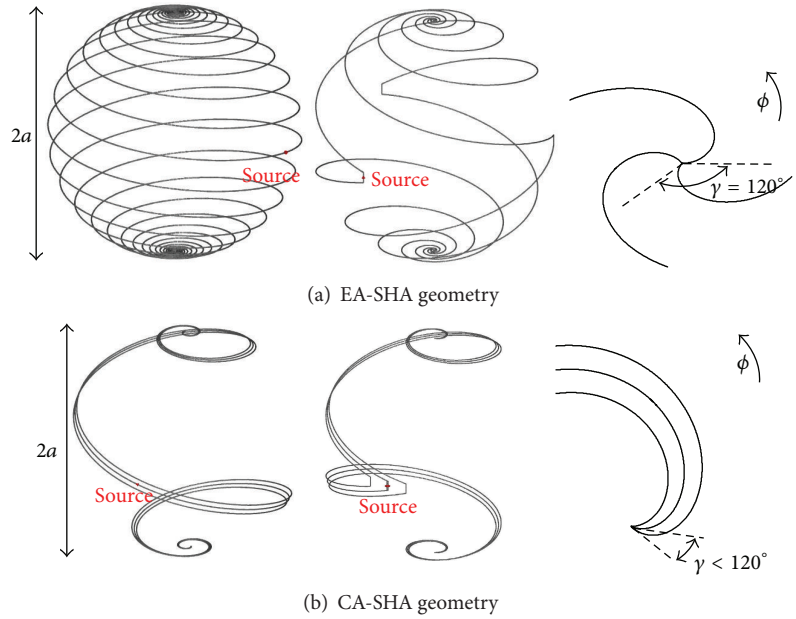

(a) EA-SHA geometry

(b) CA-SHA geometry

FIGURE 4: Examples of three-arm SHA geometries, from left to right: (a) EASS-SHA, EARS-SHA, EA spirals with difference angle γ and (b) CASS-SHA, CARS-SHA, CA spirals with difference angle γ.

a capacitor [29, page 226]. The increase of internal capacitance is emphasized the most in EARS-SHA, whereas the difference in self-resonant frequencies between single-arm and multiple-arm EARS-SHAs is the greatest (see Table 1). It can be noted that the diameter of the impedance circle in the Smith diagram decreases with the number of arms added. However, not only that this implies a higher radiation resistance, but it also implies a reduced frequency span between the two neighboring anti-resonant frequencies. This frequency interval has relatively flat radiation characteristics convenient for practical use. Concerning all examined SHA configurations, the results indicate that one must be careful with adding a large number of arms not only due to the decreasing range between the antiresonances, but also due to the increase in self-resonant frequency placing it nearer to that of the antiresonance.

Let us focus on the results of slightly modified folded SHA design used in CA-SHAs (CASS- and CARS-SHAs) in Table 1 and Figure 5. Instead of changing the antenna dimensions, or adding inductive loading to detain the resonant frequency of multiple-arm SHA near the self-resonant frequency of single-arm SHA as done in [17], we rearranged the SHA arms in order to annihilate the increased self-capacitance by bringing the arms closer to each other. This caused a more symmetrical impedance circle relative to the real axis of the Smith chart, produced even higher radiation resistance, and lowered the self-resonant frequency of multiple-arm CA-SHAs in comparison with multiple-arm EASS- and EARS-SHAs.

Now, we compare these results with the radiation resistance dependence with N_A^2 [19]. The relative deviation Δ_r of the resonant radiation resistance of each simulated multiple-arm SHA R_m^{rad} from $N_A^2 R_1^{\text{rad}}$, R_1^{rad}, being the radiation resistance of the corresponding single-arm SHA, is depicted in

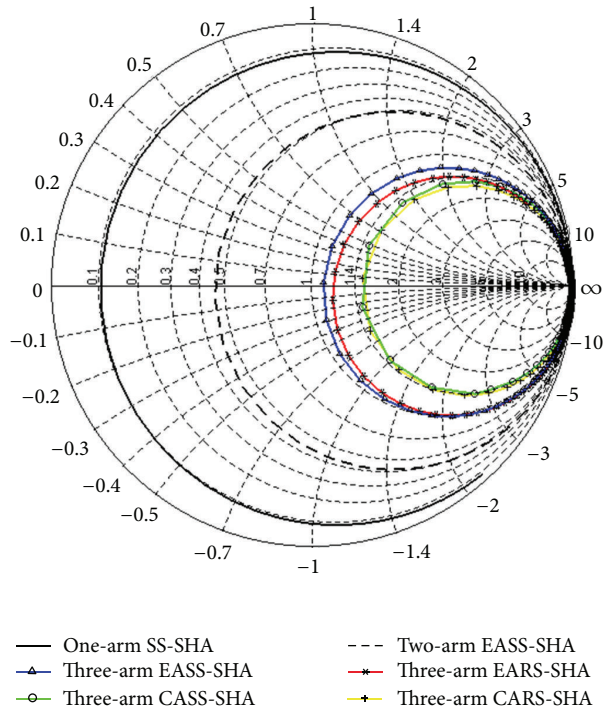

FIGURE 5: The Smith impedance diagram (normalized to 50 Ω) of one-, two-, and three-arm PEC SHAs.

Figure 6 as a function of N_A ($\Delta r = (R_m^{\text{rad}} - N_A^2 R_1^{\text{rad}})/N_A^2 R_1^{\text{rad}}$). The results show that the deviation has a positive sign and increases approximately linearly with N_A for each SHA configuration, with a steepest slope for the CARS-SHA. Among the simulated, the three-arm CASS-SHA is selected

Table 2: The three-arm SHAs basic properties.

Three-arm SHA	a (cm)	γ (°)	ψ (°)	f_{res} (MHz)	$k_{res}a$	R^{rad} (Ω)	VSWR (50 Ω)	η_{rad} (%)	α
EASS-SHA	10	120	15.9	161.5	0.34	56.44	1.18	95.5	0.36
EARS-SHA	5	120	7.2	160.4	0.17	13.98	3.00	83.8	0.45
CASS-SHA	5	10	7.5	158.8	0.17	47.73	1.23	77.4	0.40
CARS-SHA	5	15	6.2	162.3	0.17	38.90	1.34	72.4	$1.2e-4$

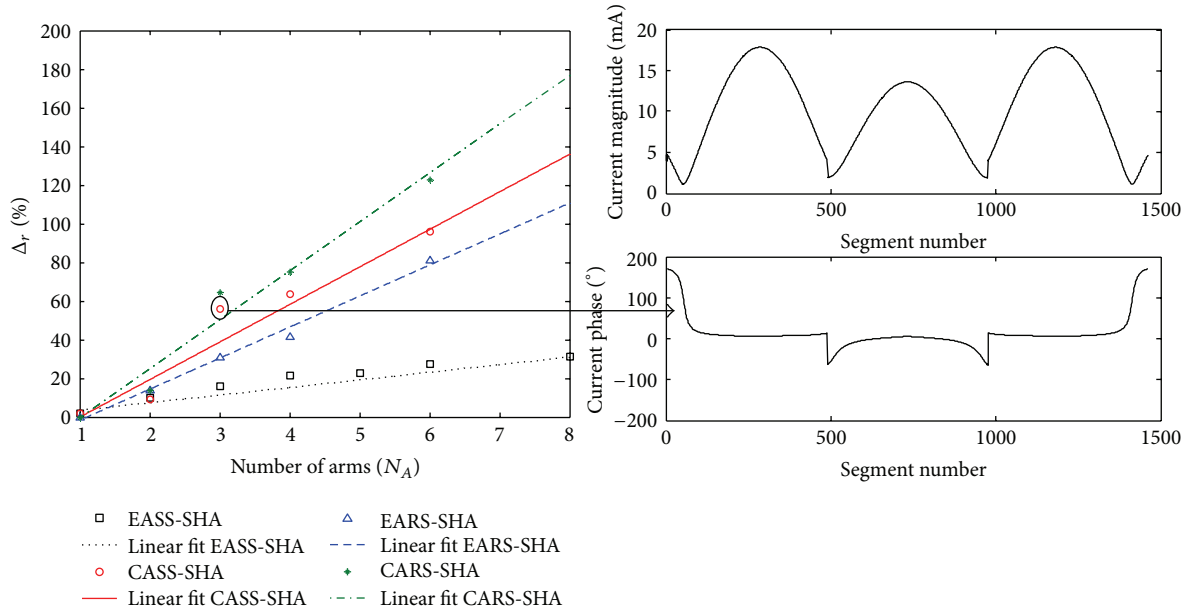

Figure 6: The relative deviation Δ_r and current distribution for three-arm CASS-SHA.

in Figure 6 in order to examine the current induced along the antenna arms. The voltage source is located in the middle of the second (center) SHA arm, Figure 4. The segment numbers indicate the order from the first to the last antenna arm. The current magnitude on the center arm is somewhat suppressed relative to the neighboring ones, while the current phase is approximately equal in all arms. Such current characteristics are observed in all examined examples of CA-SHAs.

Except for boosting the radiation properties of ESA, the folding concept is used to match the antenna to 50 Ω impedance for practical purposes [20]. In addition, the effect of lowering the angle between the arms to achieve higher antenna resistance than in commonly used folded helical antenna designs [12, 17, 20], for example, in the EASS-SHA design, can be used for the impedance match while reducing the volume of SHA. This is shown in Table 2 where we applied this effect to the SS- and RS-SHA geometries. All SHAs are made of copper wire with radius $r_w = 0.29$ mm.

In the first step, the size of the three-arm EASS-SHA was reduced to half of its volume. The radiation efficiency decreased almost 12%, and the radiation resistance dropped approximately four times due to the procedure. The wire length (i.e., the pitch angle) and the angle between the arms had to be further adjusted to achieve nearly the same self-resonant frequency and impedance match. Consequently, the radiation efficiency decreased further for a few percents. In the case of CARS-SHA, a smaller pitch was required to achieve the resonance and 50 Ω match due to increased internal capacitance in the RS-SHA geometry (see Figure 5). Compared with their single-arm SHA counterparts of equal electrical sizes, the radiation efficiencies increased to 7.0%, 19.1%, 12.7%, and 15.6% in the case of three-arm EASS-SHA of $a = 10$ cm, EARS-SHA of $a = 5$ cm, and CASS-SHA and CARS-SHA of $a = 5$ cm, respectively.

Figure 7(a) shows that high radiation resistance is achieved with reduced-size CA-SHAs (with $k_{res}a = 0.17$, where $k_{res} = 2\pi/\lambda_{res}$), as well as good impedance match to 50 Ω shown in Table 2. Also, it can be noticed that, when the SHA arms are close together, the radiation efficiency characteristic becomes distinctive in the limited region around self-resonant frequency regardless whether RS- or SS-SHA design is considered. In certain practical ESA designs for the purpose of matching, one may consider using the combination of the inductive feed and the adjustment of space between the folded antenna arms.

The results of mode ratios obtained by FEKO are given in Figure 7(b) for the three-arm CARS-, CASS-, and EASS-SHAs, compared with the analytical expression for mode ratio of single-arm SHA [13]:

$$\alpha = \frac{1}{4}(ka)^2\cot^2\psi. \quad (14)$$

Table 3: Single-arm SHA configurations' resonant properties.

One-arm SHA	a (cm)	ψ (°)	f_{res} (MHz)	$k_{res}a$	R^{rad} (Ω)	η_{rad} (%)	α
Open-ended SS-SHA	2.5	3.64	162.1	0.085	0.40	30.8	0.44
Open-ended RS-SHA	2.5	2.83	162.0	0.085	0.43	22.9	$3e-4$
Loop SS-SHA	2.5	1.95	161.9	0.085	0.38	19.9	0.14
Loop RS-SHA	2.5	1.63	160.5	0.085	0.61	20.1	$5e-5$
Loop SS-SHA with $C = 2.8$ pF	2.5	7.50	162.3	0.085	0.23	6.3	2.23

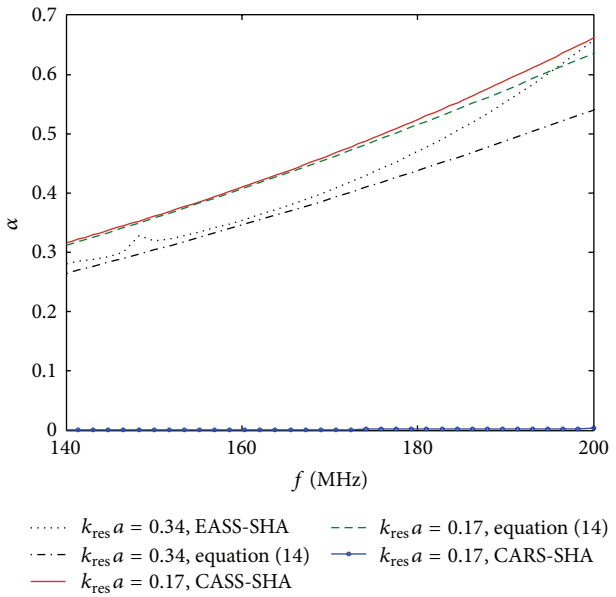

(a) Radiation efficiency

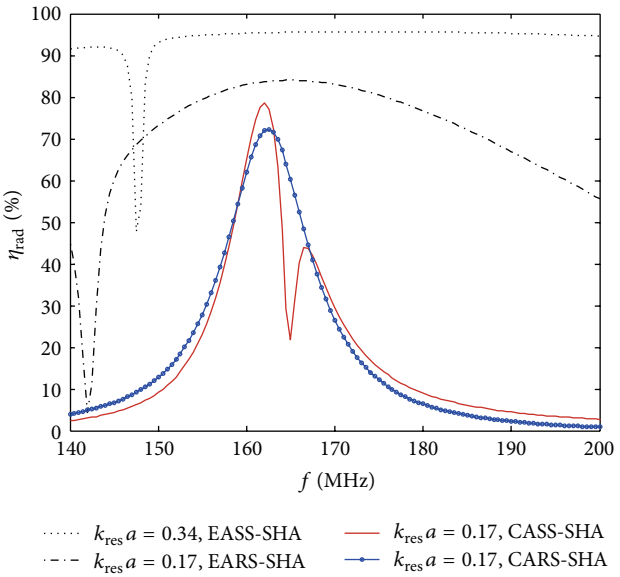

(b) Mode ratio

Figure 7: Radiation properties of examined SHAs from Table 2 versus frequency.

A fairly good agreement between the results calculated by (14) and the simulated ones for the considered three-arm SS-SHAs is achieved near the self-resonant frequency. This comparison and other SHA simulations conducted show that the folding concept does not affect the mode ratio much in the region around the self-resonant frequency. Compared with the case of CASS-SHA, the equality of TE and TM mode powers of EASS-SHA is achieved at a lower frequency. In the region around self-resonant frequency, one can notice a slight difference in mode ratio, where CASS-SHA generates somewhat stronger TE mode. This is due to the increased number of turns needed to achieve the same self-resonant frequency with the reduced antenna size [14, 17], as mentioned in Section 1. The shape of CARS-SHA is very convenient because it cancels a great deal of the lowest TE mode power, inducing an almost pure TM mode in a large frequency bandwidth. Thus, CARS-SHA presents a good candidate for the optimum SHA design, offering great possibilities in achieving a convenient mode ratio, a satisfactory radiation efficiency, and a high radiation resistance providing the impedance match.

3.2. Loop and Open-Ended SHA Configurations. Further analysis focuses on the SHAs with small or moderate radiation efficiency typical for electrically very small antennas. Table 3 shows the characteristics of different single-arm SHAs that resonate at approximately equal frequencies (as the SHAs in Table 2). These are the open-ended SS- and RS-SHAs and the loop SS- and RS-SHAs [21]. Also, the loop SS-SHA with a capacitor in series was simulated. All of the SHAs are made of copper wire with 0.29 mm radius and occupy equal spherical volumes of radius: $a = 2.5$ cm and $k_{res}a = 0.085$.

The radiation efficiencies and the mode ratios are given in Figures 8(a) and 8(b), respectively. Open-ended SS-SHA achieves the best radiation efficiency near the self-resonant frequency, and its mode ratio shows that TM mode is dominant over TE mode (but the TE mode power is not negligible). The radiation efficiency is higher than that of the open-ended RS-SHA. This is because RS-SHAs require a longer wire to achieve self-resonance at the same frequency as that of the corresponding SS-SHAs, and their loss resistance is greater. At the same time, the radiation resistances of the two remain approximately equal. However, RS-SHA (e.g., CARS-SHA) achieves very high TM mode purity in a large fractional bandwidth.

The analysis in [21] showed that short-circuiting the helical antenna ends generally expels the TE mode except at the lowest frequencies. Furthermore, the lowest anti-resonance occurs prior to the first self-resonance. Therefore, we must add more turns in order to achieve the same self-resonant frequency as that of the open-ended SHA. This is

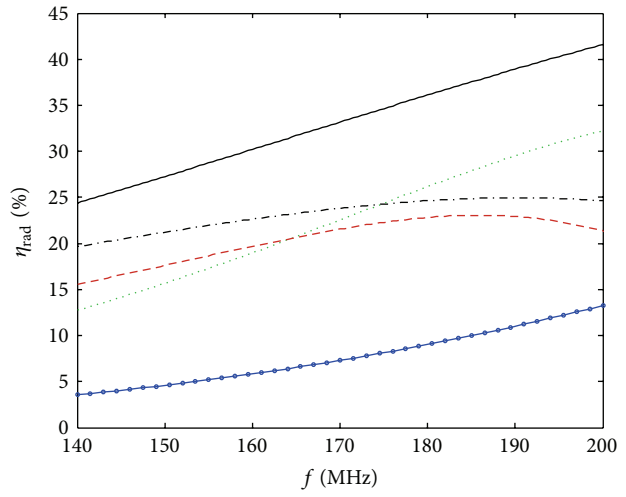

(a) Radiation efficiency

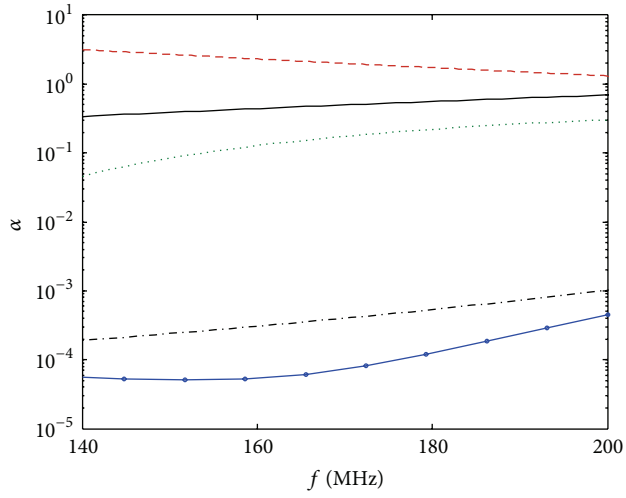

(b) Mode ratio

FIGURE 8: Radiation properties of examined SHAs from Table 3 versus frequency.

in agreement with the results for both SHA configurations, loop SS- and RS-SHAs, as they both generate somewhat lower mode ratios α than those in open-ended configurations (Figure 8(b)).

The loop SS-SHA and generally antennas with short-circuited ends offer a possibility to lower the resonant frequency by adding the capacitor in series. This is convenient due to the small additional loss (as opposed to adding the inductors), but in that case, the radiation efficiency drops significantly, and the mode ratio greatly differs from that of the self-resonant antenna. From Figure 8(b), it can be noted that for the loop SS-SHA with capacitor TE mode dominates over TM mode in the considered frequency band.

Considering that the maximum WPT performances are governed exclusively by radiation efficiency and mode ratio match between the antennas, the main conclusions of the analysis in this section can be summarized as follows.

It is shown that multiple-arm folded design of electrically small SHAs provides a means for achieving high radiation efficiency and radiation resistance near resonant frequency, whereas the mode ratio remains unaffected by adding the folded arms. The antenna resistance can be additionally boosted by varying the separation between the arms at the expense of the usable bandwidth around resonant frequency. It is noted that, for the fixed-resonant frequency, the reduction of SHA's electrical size narrows the bandwidth, lowers the radiation resistance, and also affects the mode ratio to a degree. The RS-SHAs generate almost pure TM mode providing a convenient mode ratio to be implemented in WPT when different antennas are used. The radiation efficiency and mode ratio of SS- and RS-SHAs can also be manipulated with the loop and open-ended configurations.

4. WPT Example with SHAs

In this section, the examined SHAs are considered for an assumed WPT example. It is taken into consideration that in many WPT applications a transmitter with high radiation efficiency is applied for powering small-size receivers with low or moderate radiation efficiency. Considering the TM mode purity of RS-SHAs providing the ability for a simpler mode ratio match between the antennas, three-arm CARS-SHA is chosen as the transmitting antenna. The selection of a suitable receiver SHA is obtained by calculating the term T_m by (6) for single-arm SHAs in Table 3 in the case of CARS-SHA transmitter (see Table 2).

For a given distance and an antenna orientation, PTE is maximized when $\mathbf{T}$ (or T_m) is maximized. Figure 9 shows that maximum T_m is obtained for PEC antennas with equal mode ratios. If the antennas are not equal and are made of real conductors, the maximum power transfer is achievable by means of maximizing H_{T_m} and A_{T_m}. For a given transmitter, the maximum A_{T_m} is achieved for the mode ratio mismatch $\alpha_2/\alpha_1 = 1$, or 0 dB. According to the results of T_m, the most suitable receiver is the open-ended RS-SHA. The second choice would be the open-ended SS-SHA with a slightly lower T_m, but higher radiation efficiency.

4.1. WPT Simulations. The simulations are obtained using the wire segment length of 1.74 mm with radius 0.29 mm for all of the SHAs. The load at the receiver, as well as the source at the transmitter port, is positioned in the middle of the wire (see Figure 4). Figure 10 shows the dependence of the maximum PTE at 162.3 MHz on distance calculated by (11) for different T_m. The optimal load is determined by (9) and (10) (as Z_L^{opt}) and by the Linville method [30] (as Z_{Linv}). There is an excellent agreement between the theory and the simulation. For PEC SHAs, in the RS-SHA receiver scenario, a higher PTE is achieved than in the one of SS-SHA due to a worse

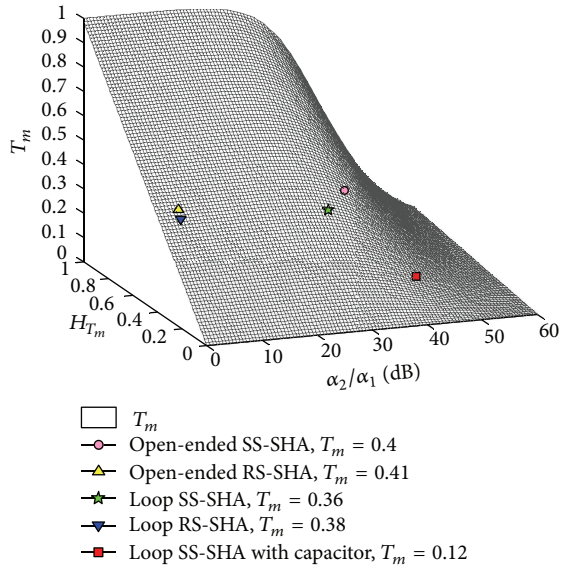

FIGURE 9: T_m versus radiation efficiency factor and mode mismatch α_2/α_1 for CARS-SHA transmitter.

mode ratio match of the latter. However, due to its higher radiation efficiency, virtually equal PTEs are obtained in both cases when copper is introduced. Therefore, it is important for small receivers to have good mode ratio matches with the transmitter.

These results obtained in VHF band can easily be translated to other frequency bands by scaling. When all of the antenna dimensions (including wire radius) are scaled while retaining the same "radiansphere", the radiation resistance and the mode ratio remain unchanged at the scaled frequency. However, the radiation efficiency changes as a consequence of the skin effect, because the loss resistance is proportional to the square root of frequency. For example, for the translation to the 40 MHz ISM band, let the antenna physical dimensions be multiplied and the frequency divided by a factor of 3.45. In that case, the calculations by (1) for the coaxial configuration of CARS-SHA and open-ended RS-SHA show that the transmission range for a 40% maximum PTE bound is increased from about 28 cm (the gap between SHAs of circa 5.5, the mean antenna radii) in VHF to 1.1 m (the gap of circa 6.5, the mean radii) in the 40 MHz ISM band.

4.2. Measurements. In order to verify the conclusions derived, we built prototypes of the selected antennas and tested them in a laboratory. Considering the fact that these SHAs are electrically very small, it was necessary to eliminate the influence of the feed cables from measurements. Therefore, monopole versions of the three-arm CARS- and open-ended single-arm RS-SHAs were made to be equivalent to the SHA dipoles listed in Tables 2 and 3, respectively. The lacquered 3-gauge copper wire was wound on a styrofoam hemisphere for the purpose. The monopole SHAs were mounted on aluminum ground-plane (2 m × 2 m × 1 mm), and the cables were connected from below the plane. VNA HP8720A was used to measure the standalone SHAs' and

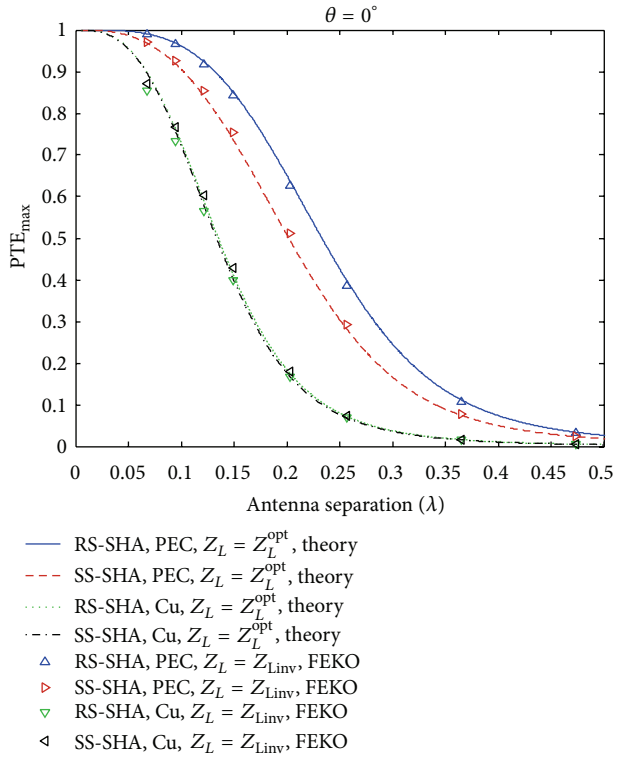

(a) Coaxial orientation

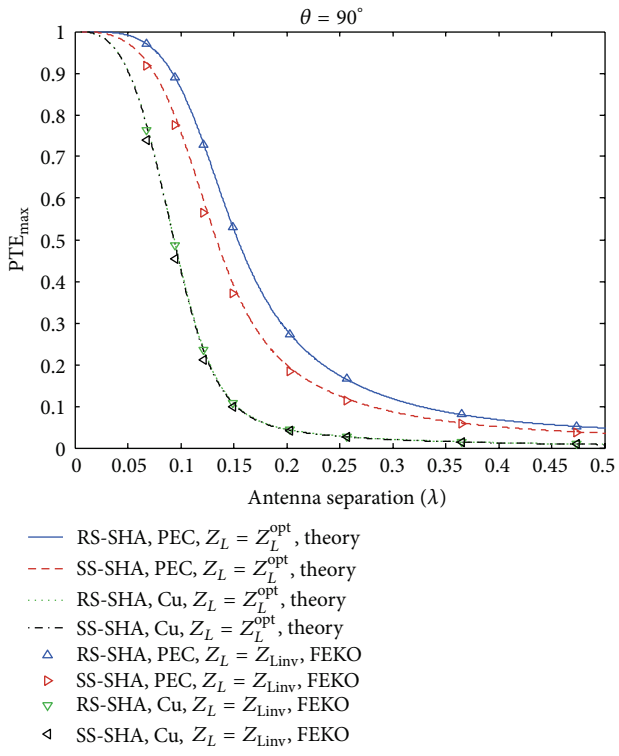

(b) Coplanar orientation

FIGURE 10: Maximum PTE in case of open-end SHA receivers with CARS-SHA transmitter.

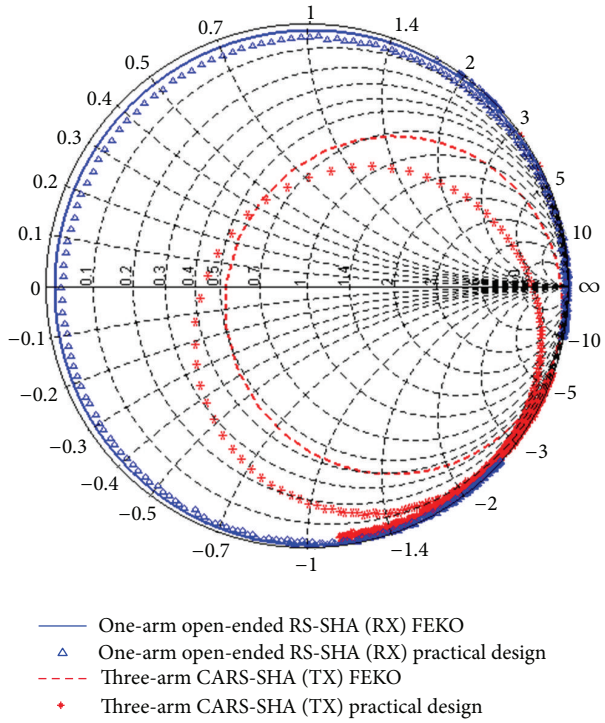

Figure 11: The 50 Ω Smith chart: standalone SHAs measurements.

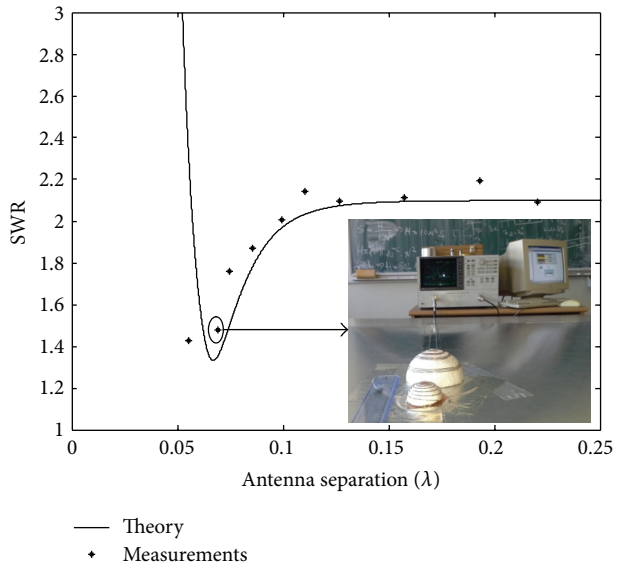

Figure 12: Comparison of measured and calculated SWR versus distance with a photo of measurement setup.

the WPT system S-parameters, after the influence of the feeding 50 Ω coaxial cables had been removed by the full two-port calibration.

As the radiation resistance of monopole SHA is reduced to a half of the one of the dipole (according to the image theory), the monopole SHA over an infinite PEC ground plane had to be simulated. Figure 11 shows the 50 Ω Smith chart where the frequency sweep is set from 135 to 195 MHz with the steps of 75 kHz and of 125 kHz for measurements and simulations, respectively. The resonant frequencies of the designed single-arm and three-arm SHAs are 163.0 MHz and 165.3 MHz, respectively. Due to the fact that these antennas are highly reactive, it was hard to achieve the exact resonant frequency as in the simulation. The measured and simulated impedance locus diameters are almost equal for both SHAs, but the one of the measured CA-SHA is slightly shifted in a clockwise direction.

The standing-wave-ratio (SWR) measured at the input of the WPT system of the two SHAs in a collinear configuration versus antenna separation is depicted in Figure 12. The selected frequency is 165.3 MHz. There is a satisfactory agreement between the theoretical results obtained using (2) and the measurements. The SWR deteriorates as the antenna separation becomes greater, and it reaches the far-field value of approximately SWR = 2.1 at a distance greater than 0.1λ.

PTE is measured according to (1) as follows:

$$\mathrm{PTE}_{\mathrm{meas}} = \frac{|s_{21}|^2}{1 - |s_{11}|^2}. \tag{15}$$

The measurements of WPT performances at 165.3 MHz depicted in Figure 13 show a fairly good agreement with simulations. The theoretical curves are obtained by applying the impedances of the designed standalone SHAs measured by VNA and the free-space impedances simulated by FEKO in (1). The simulated and measured PTEs show a very good agreement with theory even for the separations less than 0.1λ. These measurements can be fully utilized as a proof-of-concept, that is, as the validation of both theory and simulations, as well as the reliability of the scheme. The maximum PTE bound in a practical WPT system can be approached by using the antennas with radiation efficiency and mode ratio match as high as possible and by proper matching of the receiver using (9)-(10) or the Linville method, as shown in Figure 10.

Considering the fact that the proposed transmitter design is electrically very small with $k_{\mathrm{res}}a = 0.17$ and achieves $\eta_{\mathrm{rad}} = 72.4\%$ with $r_w = 0.29$ mm, there are various possibilities for boosting its radiation properties. These include the enlargement of its size and wire radius as well as adding more folded arms. A FEKO simulation shows that the radiation efficiency of the enlarged self-resonant three-arm CARS-SHA at 161.3 MHz ($\psi = 12.6^\circ$, $\gamma = 20^\circ$, and $r_w = 0.53$ mm) is 95.5% with a good impedance match to 75 Ω (75 ΩVSWR = 1.02). This would bring the maximum PTE between the two equal SHAs even closer to the theoretical bound than in [20].

5. Conclusion

The theoretical bound for WPT between two different ESAs is examined by using the antennas of reduced size, that is, limited radiation efficiency. It is shown that the practical problem of matching the impedance of reduced-size SHAs to standard transmission lines can be solved with a modified multiple-arm folded SHA design. It provides a possibility

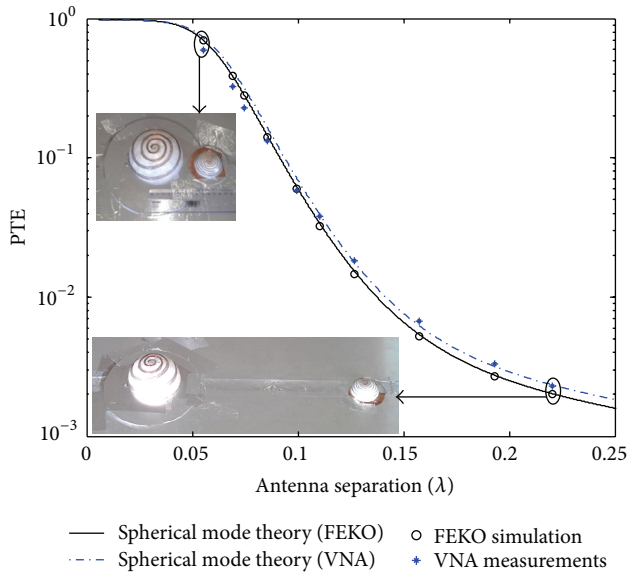

Figure 13: PTE measured between the two different SHAs and comparison between simulation and theory.

to achieve high radiation efficiency and radiation resistance higher than those in the reported literature. The theory and the simulation show that it is crucial to achieve mode ratio match between the transmitter and receiver in order to approach the maximum PTE considering WPT system of two different, matched, and electrically very small SHAs ($k_{\text{res}}a$ = 0.17 and 0.085). Proof-of-concept measurements confirm the reliability of theoretical and simulation results.

The mode ratio can be manipulated by different SHA configurations examined in the paper. It is concluded that, due to the TM mode purity, the reverse-sensed design enables easier mode matching when different SHAs are utilized at transmission and reception. However, the single-sensed one achieves higher radiation efficiency in self-resonance making it a better candidate for WPT when equal SHAs are applied in the system.

The future work on the subject should address the SHA performances when a number of receivers and multiple transmitters are applied in the same WPT network. The characteristics of the radio-channel analysis for the coupled SHA dipoles over PEC and real ground will be considered as well.

References

[1] N. Tesla, *Colorado Springs Notes 1899-1900 (With Commentaries)*, vol. 1978, Nolit, Beograd, Serbia, ed. by Marinčić A.

[2] A. Marinčić, "Nikola Tesla contributions to the development of radio," *Yugoslav IEEE MTT Chapter Informer*, no. 1, pp. 10–12, 1994.

[3] N. Tesla, "Means for increasing the intensity of electrical oscillations," USPO Pat. No. 685, 012, 1901.

[4] W. C. Brown, "The history of power transmission by radio waves," *IEEE Transactions on Microwave Theory and Techniques*, vol. 32, no. 9, pp. 1230–1242, 1984.

[5] H. Matsumoto, "Research on solar power satellites and microwave power transmission in Japan," *IEEE Microwave Magazine*, vol. 3, no. 4, pp. 36–45, 2002.

[6] N. Shinonhara, "Power without wires," *IEEE Microwave Magazine*, vol. 12, no. 7, pp. 564–573, 2011.

[7] A. Kurs, A. Karalis, R. Moffatt, J. D. Joannopoulos, P. Fisher, and M. Soljačić, "Wireless power transfer via strongly coupled magnetic resonances," *Science*, vol. 317, no. 5834, pp. 83–86, 2007.

[8] H. A. Haus and W. Huang, "Coupled-mode theory," *Proceedings of the IEEE*, vol. 79, no. 10, pp. 1505–1518, 1991.

[9] S. Ahn and J. Kim, "Magnetic field design for high efficient and low EMF wireless power transfer in on-line electric vehicle," in *Proceedings of the 5th European Conference on Antennas and Propagation (EUCAP '11)*, pp. 4148–4151, April 2011.

[10] S. I. Park, "Enhancement of wireless power transmission into biological tissues using a high surface impedance ground plane," *PIER*, vol. 135, pp. 123–136, 2013.

[11] J. Lee and S. Nam, "Fundamental aspects of near-field coupling small antennas for wireless power transfer," *IEEE Transactions on Antennas and Propagation*, vol. 58, no. 11, pp. 3442–3449, 2010.

[12] H. B. Riblet, "A broad-band spherical satellite antenna," *Proceedings of the IRE*, vol. 48, pp. 631–635, 1960.

[13] K. K. Mei and M. Meyer, "Solutions to spherical anisotropic antennas," *IEEE Transactions on Antennas and Propagation*, vol. 12, no. 4, pp. 459–463, 1964.

[14] H. A. Wheeler, "The spherical coil as an inductor, shield, or antenna," *Proceedings of the IRE*, vol. 46, no. 9, pp. 1595–1602, 1958.

[15] S. R. Best, "The radiation properties of electrically small folded spherical helix antennas," *IEEE Transactions on Antennas and Propagation*, vol. 52, no. 4, pp. 953–960, 2004.

[16] H. L. Thal Jr., "New radiation Q limits for spherical wire antennas," *IEEE Transactions on Antennas and Propagation*, vol. 54, no. 10, pp. 2757–2763, 2006.

[17] S. R. Best, "The performance properties of electrically small resonant multiple-arm folded wire antennas," *IEEE Antennas and Propagation Magazine*, vol. 47, no. 4, pp. 13–27, 2005.

[18] Z. Blažević and M. Škiljo, "Optimal design for a class of spherical helical antennas applied in wireless transmission of energy by resonant coupling," in *Proceedings of the 20th International Conference on Software, Telecommunications and Computer Networks (SoftCOM '12)*, pp. 1–4, Split, Croatia, September 2012.

[19] S. Lim and H. Ling, "Design of thin, efficient, electrically small antenna using multiple foldings," *Electronics Letters*, vol. 42, no. 16, pp. 895–897, 2006.

[20] I. J. Yoon and H. Ling, "Realizing efficient wireless power transfer using small folded cylindrical helix dipoles," *IEEE Antennas and Wireless Propagation Letters*, vol. 9, pp. 846–849, 2010.

[21] Y. Tak, J. Park, and S. Nam, "The optimum operating frequency for near-field coupled small antennas," *IEEE Transactions on Antennas and Propagation*, vol. 59, no. 3, pp. 1027–1031, 2011.

[22] E. Almajali, D. McNamara, and D. Lee, "Using electromagnetic simulation code FEKO as a numerical laboratory in antenna engineering," in *Proceedings of the 14th International Symposium on Antenna Technology and Applied Electromagnetics and the American Electromagnetics Conference (ANTEM/AMEREM '10)*, pp. 1–4, July 2010.

[23] H. A. Wheeler, "Fundamental limitations of small antennas," *Proceedings of the IRE*, vol. 35, no. 12, pp. 1479–1484, 1947.

[24] L. J. Chu, "Physical limitations of omni-directional antennas," *Journal of Applied Physics*, vol. 19, no. 12, pp. 1163–1175, 1948.

[25] W. W. Wasylkiwskyj and K. W. Kahn, "Scattering properties and mutual coupling of antennas with prescribed radiation pattern," *IEEE Transactions on Antennas and Propagation*, vol. 18, no. 6, pp. 741–752, 1970.

[26] J. B. Andersen and R. G. Vaughan, "Transmitting, receiving, and scattering properties of antennas," *IEEE Antennas and Propagation Magazine*, vol. 45, no. 4, pp. 93–98, 2003.

[27] A. Safaai-Jazi, "Radiation characteristics of a spherical helical antenna," *IEE Proceedings-Microwaves Antennas and Propagation*, vol. 143, no. 1, pp. 7–12, 1996.

[28] M. Škiljo and Z. Blažević, "Investigation of electrically small monofilar spherical helical antenna used for mid-range wireless power transfer," in *Proceedings of the 35th International Convention of Information Communication Technology, Electronics and Microelectronics (MIPRO '12)*, pp. 247–251, Opatija, Croatia, May 2012.

[29] R. Beringer, "Resonant cavities as microwave circuit elements," in *Principles of Microwave Circuits*, McGraw-Hill, New York, NY, USA, 1948.

[30] C. A. Balanis, *Antenna Theory: Analysis and Design*, John Wiley & Sons, New York, NY, USA, 2nd edition, 1997.